Jour. Fac. Sci., Hokkaido Univ., Ser. VII (Geophysics), Vol. 10, No. 2, 189-223, 1997.

Characteristics of Clouds and Cloud Clusters Obtained by Radar and Satellite Data during the TOGA-COARE IOP

Md. Nazrul Islam*, Hiroshi Uyeda and Katsuhiro Kikuchi

Division of Earth and Planetary Sciences, Graduate School of Science, Hokkaido University, Sapporo 060, Japan

(Received December 9, 1996)

Abstract

In order to understand the general characteristics of the clouds and cloud clusters over the western Pacific warm pool, analyses were performed for 2 days (Nov. 11-12, 1992) during the TOGA-COARE IOP, on radar and satellite data when Keifu Maru (a Japanese research vessel) was cruising in the IFA region. Doppler radar data collected on Manus Island were also analyzed to understand the vertical structure of tropical clouds. A modified CST (Convective Stratiform Technique) was used to analyze GMS-IR data to compare the cloud characteristics with those of radar analysis.

Using Keifu Maru radar, the lifetime of the echo elements of isolated echoes and nonisolated echoes was calculated. The elements of nonisolated echoes were found to last longer (1-5 hours) than the elements (20 minutes to 1 hour) of isolated echoes. This long lasting quality of the individual elements supported the nonisolated (sub-system) echo in its long life. This also implies that long lasting (~13 hours) sub-system is essential to the formation and maintenance of a system while each sub-system has to be composed of a number of long-lived elements. In contrast, short-lived elements are organized to form isolated echoes (~5 hours) which die down fast and do not take part in the formation of the sub-system or the system. The long-lived nonisolated echo was analyzed to have traversed a distance (~350 km) longer than that (~155 km) of the short-lived isolated echo even though the area and moving speed were almost the same. Importantly, the duration of the developing stage lifetime was calculated at approximately one-third of the duration of the total lifetime for both isolated and nonisolated echoes.

The convective rainfall amount determined by the CST was found to be lower than that determined by Keifu Maru radar, even though the area was comparable. The present analysis recognized that this underestimate came from the low rain rate calculated by the CST and the high intensity of Keifu maru radar, and strongly suggested the need to assign the CST rain rate from radar data. The results of precipitation determined by the CST and three radars indicated the necessity of adapting the CST for TOGA-COARE convection in order to obtain better agreement between the results determined by the CST and radar.

* Present Affiliation : Department of Physics, Bangladesh University of Engineering and Technology, Dhaka-1000, Bangladesh

1. Introduction

The study of tropical clouds is important because it has an impact on radiative fluxes, atmospheric latent heating, and fresh water flux into the ocean. Furthermore, the fresh water flux from precipitating clouds plays an important role in the enhancement of the tropical sea surface temperature (Webster and Lukas, 1992). One of the principal driving mechanisms of the atmospheric general circulation is that the surrounding environment is modified through the release of latent heat associated with the tropical convection. Because the Pacific warm pool occupies about 20% of the surface of the earth, its variation can ultimately modify the large-scale circulation of the surrounding ocean and atmosphere. It is therefore necessary that we study tropical meteorology to understand the role of the tropical convection in the climate. An observational and modeling program, the Tropical Ocean Global Atmosphere (TOGA) Coupled Ocean-Atmosphere, Response Experiment (COARE) has been designed to gain a clear understanding of the global climate, the ENSO (El Niño-Southern Oscillation) phenomenon, and the inter-seasonal variability of the coupled atmosphere-ocean system (Webster and Lukas, 1992). Among the many objectives of the TOGA-COARE, the investigation of the properties of clouds and precipitation in the region are important targets of study.

In order to understand the organization mechanism of the tropical mesoscale convective systems (MCSs) which have often been referred to as "cloud clusters" (e.g., Houze and Betts, 1981), analysis detailing the internal structure throughout their lifetime is needed. Current analyses of cloud clusters during the TOGA-COARE Intensive Observation Period (IOP) have been reported in several works. The internal structure of a cloud cluster composed of four subsystems was analyzed by Mori (1992) and suggests the necessity of a detailed investigation of cloud cluster sub-systems to reveal the organization mechanism of cloud clusters. A few observational results revealed the horizontal and vertical structures, and the life cycle of the clouds in the TOGA-COARE domain during the IOP (Mori, 1995; Uyeda et al., 1995; Takahashi and Uyeda, 1995; Satoh et al., 1995; Kikuchi and Uyeda, 1996). It is also necessary that we understand the life cycle of the individual radar echo cell, the isolated echo, and the nonisolated echo. Moreover, we have to know how the clouds and cloud clusters are formed; i.e., the internal structure and interactions within and between the MCSs.

One may be interested in the time duration of the early development of clouds i.e., the formative stage of the cloud or the time of the formation of the

anvil cloud. This work revealed these properties by using a large coverage of Keifu Maru C-band radar data in addition to the analysis of satellite data.

Precipitation from the MCSs, as typical of the warm pool, has both convective and stratiform components (Houze, 1977 ; Leary, 1984). Because of the lack of conventional cloud and precipitation observations over the ocean, the use of satellite data is clearly desirable. Moreover, radar data results in a clear determination of the precipitation amounts associated with shallow and isolated convection. Therefore, the use of radar data to calibrate the results of high spatial resolution satellite data will result in the classification and quantification of all types of clouds in the tropics. Performing the calibration where radar data is available will be useful for a large domain using only satellite data. Mori (1995) described the mesoscale precipitating systems using Keifu Maru radar data during the TOGA-COARE IOP. His analysis, however does not cover the comparative results between the radar and satellite analyses. This analysis covered the comparative study between radar and satellite analyses. Furthermore, the current analysis focused on the comparative study between the isolated and nonisolated echoes to reveal the organization mechanism of isolated and nonisolated echoes.

The important thing was to locate or construct a sound method for the analysis of satellite data. In this analysis, the Convective Stratiform Technique (CST) algorithm was chosen because it was tested for the analyses of Florida convection (Adler and Negri, 1988 ; hereafter AN88), Winter Monsoon Experiment (WMONEX) cloud clusters (Goldenberg et al., 1990 ; hereafter GHC90) and TOGA-COARE cloud clusters (Kikuchi and Uyeda, 1996). AN88 obtained a general agreement between radar and rain-gauge observed rainfall. GHC90 obtained similar results in radar value in its early period, before the system moved out of range of the coastal radar. Kikuchi and Uyeda (1996) applied the GHC90's CST on the cloud clusters observed in Manus Island during the TOGA-COARE IOP. They reported disagreements between the results of radar and the CST. This implies that the properties of the convection in the TOGA-COARE domain are somewhat different from the properties of Florida convection or WMONEX convection. Sophisticated tasks were incorporated to detect what and where the cause is in the CST calculations, that results in the disagreement between the results of radar and satellite observations. By applying the GHC90's CST to GMS-4 IR imagery and comparing the results with those of three radars, the present analysis is able to recognize the parameters of the CST which have to be modified for the TOGA-COARE convection.

In this paper, the characteristic features of the isolated and nonisolated

echoes were analyzed at various stages of their lifetimes. Radar and GMS-4 IR data were utilized to reveal the cloud properties in the lower-level and upper-level. One of the main objectives of this paper is to detect the cause of the disagreement between the results of radar and satellite (CST), as reported by Kikuchi and Uyeda (1996), for the TOGA-COARE convection.

2. Data used to analyze

Data used in this study was mainly Keifu Maru radar data. The research vessel "Keifu Maru" which was anchored in the TOGA-COARE Intensive Flux Array (IFA), carried a C-band (wavelength : 5 cm) conventional weather radar covering 250 km in radius (Fig. 1). The outline of the Keifu Maru radar system is described in Mori (1992). The ship track of the Keifu Maru on the TOGA-COARE cruise is described in Mori (1995). Reflectivity data digitized over a 2.5 km mesh was obtained over a 500 km $\times$ 500 km area covering a large part of the IFA. The 7.5 minute interval PPI data with an elevation angle of 0.0° from November 11 to November 12, 1992 was utilized in the present study.

In the analysis of Keifu Maru data, a pattern matching technique was used. In order to calculate rainfall amount from radar data, reflectivity was converted into rain rate by using the Z-R relationship. This analysis adopted the standard Z-R relationship given by

$$Z = BR^{\beta} \tag{1}$$

where Z is the radar reflectivity factor in $mm^6\ m^3$, and R is rain rate in mm h^{-1}, and B and β are positive numbers determined empirically. The most popular values of 200 and 1.6 for B and β respectively, determined by Marshall and Palmer (1948), were adopted in this analysis.

The rain rate obtained from the average value of $>$40dBZ in a PPI scan was used as the convective rain rate of this study. The stratiform rain rate was calculated from the average rain rate $\leq$40dBZ in a PPI scan. The determination of 40dBZ as a threshold reflectivity for Keifu Maru radar to divide convective and stratiform components is described in Islam (1996).

The details of the X-band Doppler radar (wavelength : 3.2 cm) observation on Manus Island (2 S, 147 E ; Fig. 1b) for two and a half months from Nov. 12, 1992 is described in Uyeda et al. (1995). The Doppler radar of the Hokkaido University Meteorological Laboratory (HUML) was installed at Nabu (right panel). The Doppler radar of the Institute of Low Temperature Science (ILTS) was installed at Momote. The distance between the two radar sites was $\sim$18

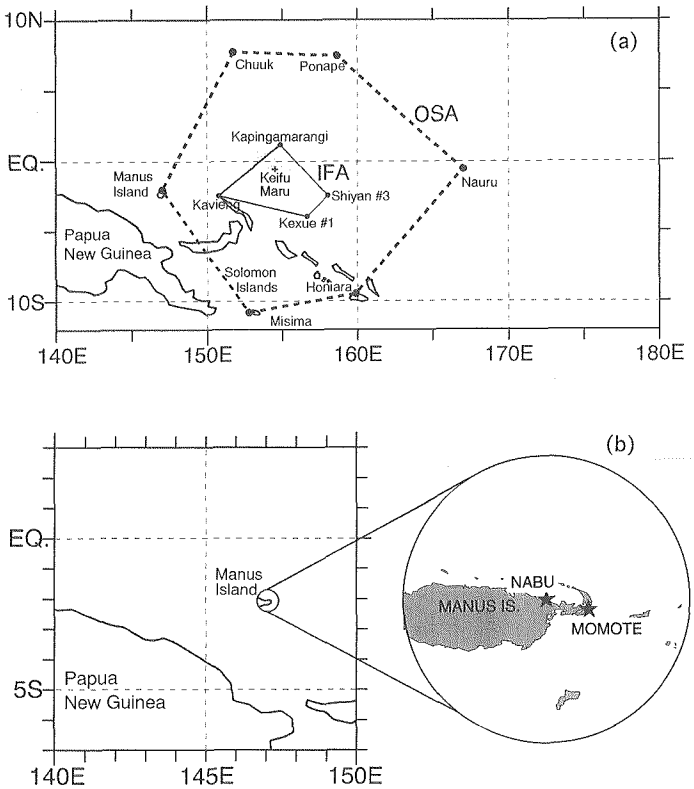

Fig. 1. a) Location of the radar observation in the TOGA-COARE domain. The outer sounding array (OSA) and the intensive flux array (IFA) are outlined. Keifu Maru is located (+ mark) at the northern part of IFA covering 250 km in radius (shaded). b) Two Japanese Doppler radars were installed in Manus Island. The HUML radar is installed at Nabu and the ILTS radar is installed at Momote. The distance between Nabu and Momote is about 18 km.

km. The observation range of every radar was 60 km in radius. Doppler radars provided the data of reflectivity and Doppler velocity. The operation modes were selected in PPI and RHI (Range Height Indicator) scans. Volume scans of PPIs were obtained at 15 minute intervals. Within a 15 minute interval, several RHI scans were performed intermittently. In the present study, PPI scan data was used to estimate rainfall amount. The RHI scan data was used to analyze the vertical structure of the significant echoes.

Doppler radar data was mainly used to analyze the vertical structure of the echo and wind field by using RHI scans assuming that the clouds to have two-

dimensional structures. The cloud top height was calculated by assuming that the height estimated from the Doppler velocity pattern of HUML radar was close to the cloud top height. The cell top height was calculated at different threshold reflectivities starting from ≥19dBZ. In the analysis of PPI data, the estimation of echo area started at ≥19dBZ and the rain rate was calculated by using the same Z-R relation as used for Keifu Maru radar.

Satellite data of GMS-4 IR on CD-ROM, 0.1° mesh of hourly T_{BB} was utilized. The hourly GMS IR data was processed specially for the TOGA-COARE IOP and was provided by Dr. Nakazawa, JMA (Japan Meteorological Agency). Suitable analysis was performed on the GMS IR equivalent black body temperature (T_{BB}) data to distinguish convective and stratiform cloud components and quantify the rainfall amounts contributed by each component.

The analysis procedure of satellite data was similar to that described by GHC90 which is modified for WMONEX. They followed the technique proposed by AN88. In order to distinguish between convective and stratiform components of MCSs, the technique used was the Convective Stratiform Technique (CST), derived by AN88 for the second Florida Area Cumulus Experiment (FACE). Two successful analyses using the CST encouraged its use in the TOGA-COARE domain. It should be noted that Kikuchi and Uyeda (1996) analyzed three cases by using GHC90's CST during the TOGA-COARE IOP. They tested the CST algorithm on data from the GMS-4 and compared the results with that of Doppler radar data collected in Manus Island. They reported the disagreement between the rainfall amounts determined by the CST and radar. However, the percentage of the convective and stratiform rainfall amounts determined by the CST for Case 2 of Kikuchi and Uyeda (1996) was satisfactory when compared with the other works. The question thus arises whether the GHC90's CST is applicable or not for the TOGA-COARE convection. The current work clearly demonstrates the need of the modification of GHC90's CST for the TOGA-COARE convection. The adaption procedure of the CST is described in a subsequent paper (Islam, 1996).

Environmental conditions during the observations were derived from sounding data. Sounding data were available for Kapingamarangi, Kavieng and on board the Keifu Maru to know the environmental condition of IFA region during the observation period.

3. Results

3.1 *Case 1 : Life cycle of a quasicircular isolated radar echo (November 11-12 in IFA region)*

The organization and life history of a quasicircular short-lived (~5 hours) isolated radar echo was analyzed in the Keifu Maru radar coverage. This echo consists of seven individual small echo cells and four fragments. The first echo cell was identified at 95 km south and 245 km west from the radar center (0.53 S, 155.32 E) at 2122 GMT on November 11. The other cells were born in their respective times and merged with the first cell to form the quasicircular echo at about 0004 GMT on November 12, as shown in Fig. 2. The analyzed echo is denoted by the solid line and the movement direction is represented by the solid arrow.

The details of the echo patterns and evolution of quasicircular isolated echo are shown in Fig. 3. Radar location of the respective time is shown by an inner-dot double circle at 30 minute intervals. PPI reflectivity contours are drawn for 20 dBZ (outer), 35 dBZ and 45 dBZ (inner). Two echo cells a1 and a2 were identified at 2134 GMT on November 11. Their next locations were traced after 30 minutes at 2204 GMT and so on. We see that a1 moved SE and a2

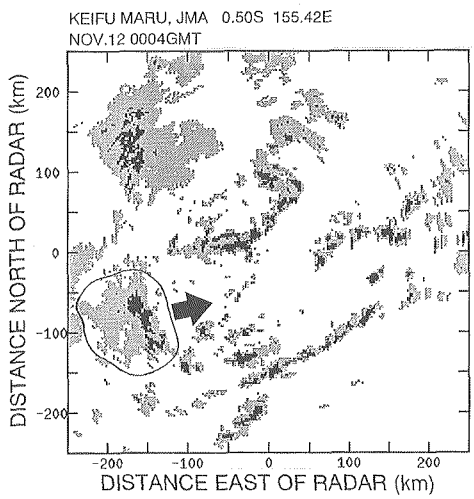

Fig. 2. Keifu Maru PPI image at 0004 GMT on Nov. 12, 1992. An isolated quasicircular short lived echo is identified by solid line. The arrow represents its movement direction. Black and gray represent echo area above and below 40 dBZ respectively.

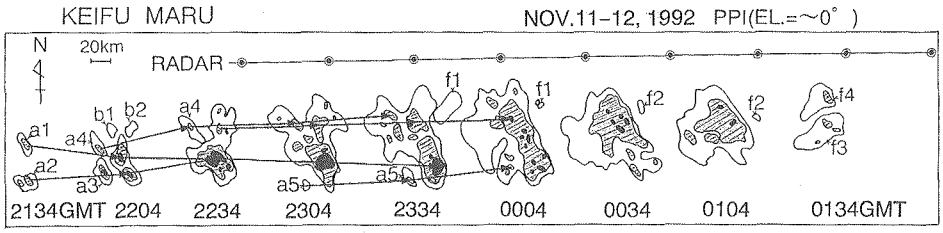

Fig. 3. Echo patterns and evolution of quasicircular isolated echo. Contours of radar echoes are drawn for 20dBZ (outer most), 35dBZ, and 45dBZ (inner) respectively. The solid line with arrows indicates the propagation speed and direction. The symbol a's and b's are used to label the echo elements. The fragments are represented by f's. The inner-dot double circles represent the center of radar location is consecutive 30 minute interval PPI images.

moved ENE, and they combined at 2204 GMT. This combined form of the cells (a1 and a2) is called a main echo. Four cells b1, b2, a3, and a4 were identified at this time and all of them merged with the pre-combined echo (main echo) at the same time. Another new cell a5 was born at 2304 GMT on November 11 and merged at 0004 GMT on November 12. It is obvious that this new cell was born in the N/NE and S/SW flanks of the main echo. In the dissipating stage, the echo showed maximum area and few fragments (labeled f's) were separated from the main echo. At the time of disappearance it had only two fragments. The echo disappeared at around 0220 GMT on November 12. This quasicircular short-lived isolated echo traversed a distance about 155 km in its lifetime.

The upper panel of Fig. 4 shows the life cycle, merging and fragmentation processes of the isolated echo corresponding to Fig. 3. All of the new cells (a's and b's) merged with the main echo, and the fragments (f's) separated from the main echo. The total echo showed its maximum area 6.5×10^4 km^2 and lasted about 5 hours. Most of the new cells were born and merged in the early developing stage which lasted about one-third of the total lifetime. This one-third time duration of the developing stage is related to the warm precipitation. Moreover, the same duration of the developing stage was found by Young et al. (1995) by using the data collected by research vessel Moana Wave during the TOGA-COARE IOP.

To understand the activeness of the echo at different stages, the growth rate of the echo was examined by measuring the area increase rate with steps (in time). An area increase rate corresponding to the upper panel of Fig. 4 is represented in the lower panel of this figure. During the total lifetime of the echo, a 15 minute interval PPI scan data ($\geq$20 dBZ) was used to calculate the

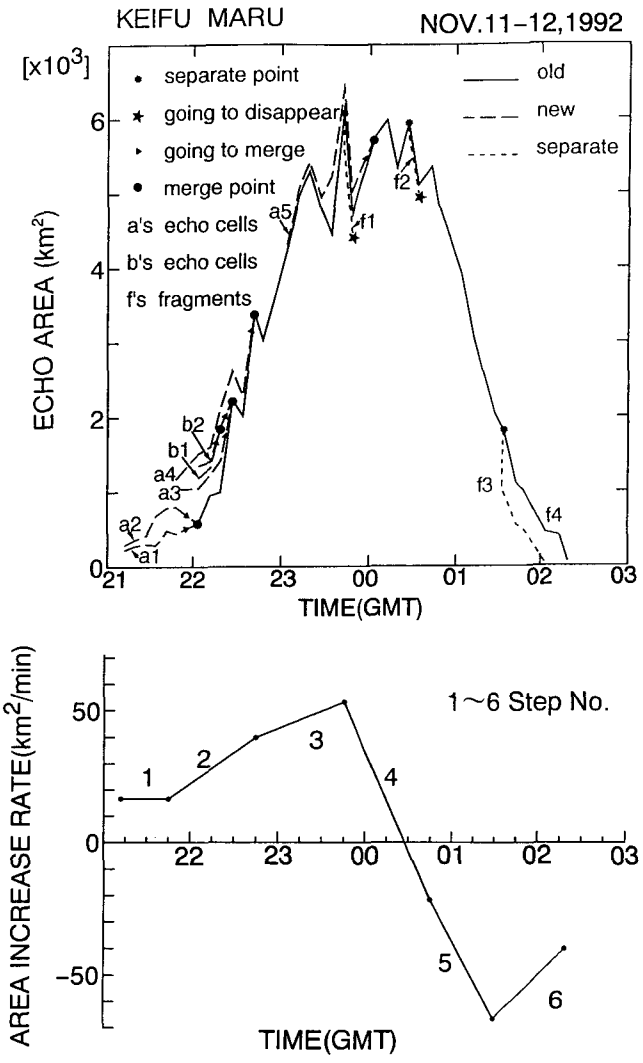

Fig. 4. Time sequence of the echo area (upper panel) corresponding to Fig. 3. The outer line represents the total echo area (≥20dBZ) at the respective time. The symbols are same as Fig. 3. The lower panel represents the echo area increase rate corresponding to upper panel. Step number represents the strength of the growth rate calculated from 7.5 minute interval PPI scan data.

steps of the area increase rate. At the first step it was 17 km²/min and increased rapidly with time in step 2. At step 3 it was at its maximum (53 km²/min) and started to decrease at step 4. The maximum decrease rate was 66 km²/min at step 5 and after that it disappeared. The rapid increase and fast decrease of area increase rates clearly reveal the reasons of the short-life of the isolated echo. The total life history of each echo cell and total echo is shown in Table 1 (section *4.1*).

3.2 Case 2 : Squall line-like nonisolated radar echo (November 11-12 in IFA region)

The organization and life history of a squall line-like (SLL) long-lived (~13 hours) radar echo was analyzed on November 11-12, 1992. This long lasting and intensive (in dBZ) SLL echo consists of six individual small echo cells. The first echo cell was identified at 150 km west and 185 km south from the radar center (0.58 S, 155.33 E) at 1904 GMT on November 11, 1992. The other cells were born in their respective times and merged with the first cell to form the SLL echo at 0204 GMT on November 12, as shown in Fig. 5.

Figure 6 represents the detailed structure and evolution of the long lasting SLL echo. Four echo cells a1, a2, a3, and b1 were identified at 2104 GMT on November 11 at different locations. Their locations were traced after 30 minutes at 2134 GMT and so on. All of the echo cells moved to the ENE. Two

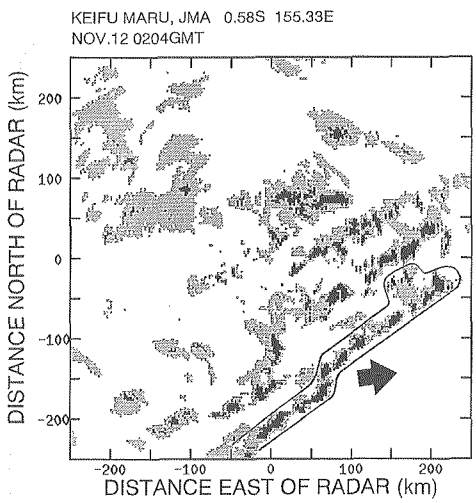

Fig. 5. Same as Fig. 2 except for a squall line-like (SLL) nonisolated echo at 0204 GMT on Nov. 12, 1992.

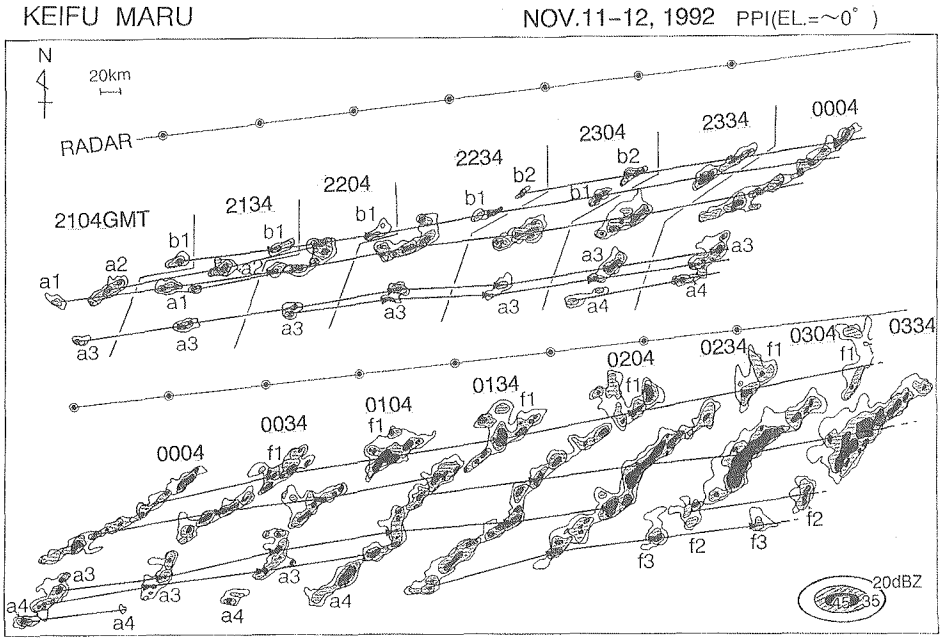

Fig. 6. Same as Fig. 3 except for a squall line-like nonisolated echo.

cells, named a1 and a2, combined at 2204 GMT. This combined echo of a1 and a2 is called the main echo. A new cell b2 was born at 2234 GMT in the NE flank of the pre-combined (main) echo. The combination of b1 and b2 joined with the main echo at 0004 GMT on November 12 and started to form the line echo. Another new echo a4 was identified in the SW flank of the main echo already at 2304 GMT on November 11, and thus the chain continued. The maximum horizontal dimension of the SLL echo was about 340 km in length at 0204 GMT on November 12. During its traversed path (~350 km), a few of the fragments (f's) separated from the main echo at their respective times. A large fragment f1 (~60 km in length) and the main echo were out of radar range after 0245 GMT and 0345 GMT respectively. However, it was possible to analyze the total life history of this SLL echo by using satellite data which will be described in section 3.4.

The upper panel of Fig. 7 shows the life cycle, merging and fragmentation processes of the SLL echo corresponding to Fig. 6. A group of the identified echo cells merged and left the main echo at their respective times. The vertical line at 0245 GMT on November 12 represents the time after which a large

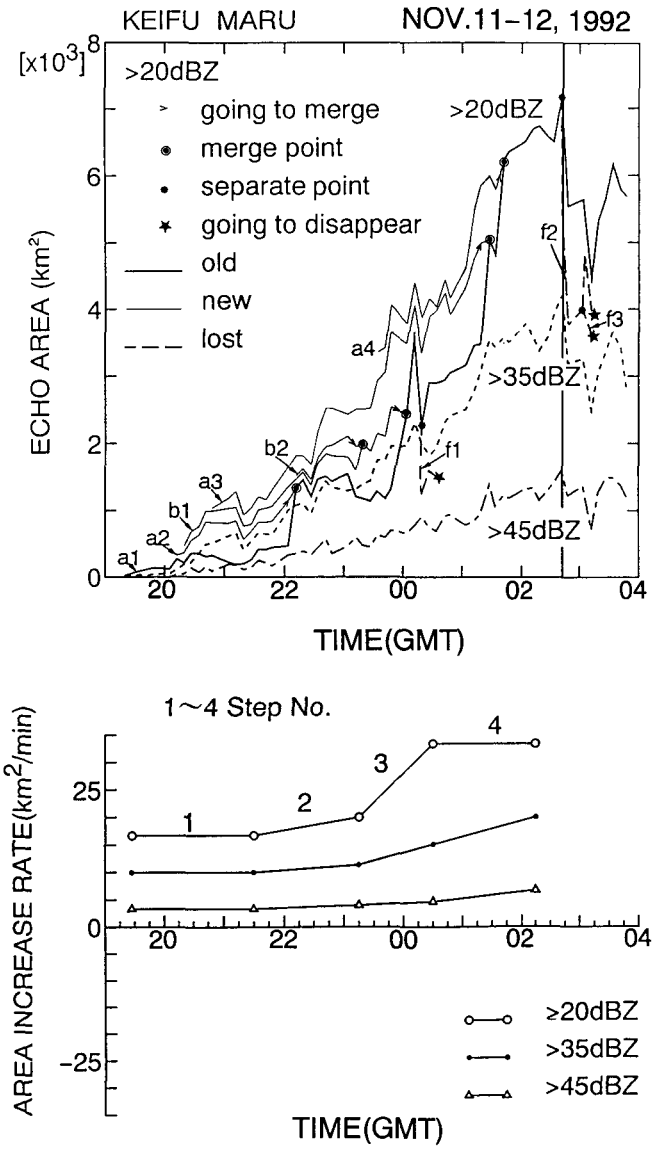

Fig. 7. Same as Fig. 4 except for a squall line-like (SLL) nonisolated echo. Thin vertical line (upper panel) represents that the echo is partly out of radar range after this time.

fragment f1 was out of radar range. The echo area suddenly decreased at 0254 GMT. The actual phenomena were examined in the GMS imagery using the CST analysis.

The area increase rate corresponding to the upper panel of Fig. 7 is shown in the lower panel of this figure. At the first step this rate was 17 km^2/min ($\geq$20 dBZ) and increased gradually with time. At step 3 the rate suddenly rose to 33 km^2/min. This sudden increase indicates that the SLL echo changed its status from a convective component to a stratiform one. At step 4 the area increase rate was almost static, this indicates that the SLL echo had reached its maximum dimension in coverage of area. Therefore, we have to believe that the SLL echo was either in a dissipating stage or moving toward a dissipating stage. The increase mode for >35 dBZ and >45 dBZ lines indicates the intensity and long life of the SLL echo. However, through examination of hourly GMS-IR data, this SLL echo was found to last approximately 13 hours and traverse a distance nearly 350 km in its lifetime. It should be noted that this type of range limitations when an echo is out of radar range can be overcome by using GMS (CST analysis) data for high spatial and temporal resolutions. In contrast, the area increase rate of the nonisolated SLL echo (Case 2) was slower than that of isolated echo (Case 1). Therefore, we may conclude that the long-lived nonisolated echo developed more slowly than the short-lived isolated echo. This is one reason the former lasted longer.

It is quite difficult to reveal the formation mechanism of the analyzed cases using only PPI scan data as collected by Keifu Maru radar. In the next section, a few cases will be analyzed using Doppler radar data collected on Manus

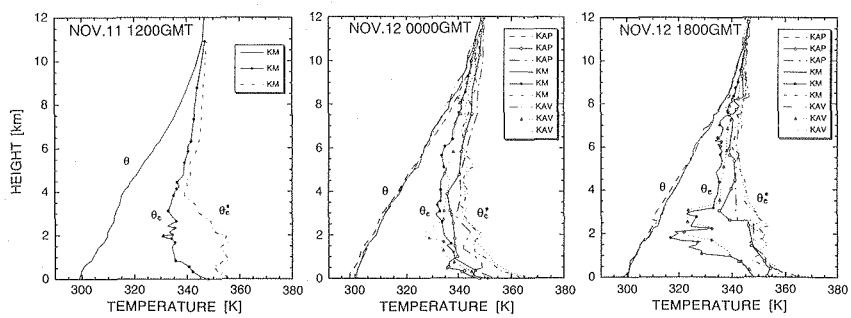

Fig. 8. Vertical profiles of potential temperature (θ), equivalent potential temperature (θ_e) and saturation equivalent potential temperature (θ_e*) deduced from soundings at three points: Keifu Maru (KM), Kapingamarangi (KAP), and Kavieng (KAV).

Island. Sounding data was used to see the environmental condition during the above cases. The potential temperature (θ), equivalent potential temperature (θ_e) and saturated equivalent potential temperature (θ_e^*) for all of Keifu Maru (KM), Kapingamarangi (KAP) and Kavieng (KAV) sounding points are shown in Fig. 8. Before the formation of the above cases (Case 1 and Case 2); at 1200 GMT on November 11, unstable condition was observed in the mid-level on board the Keifu Maru (no data for other points). During the mature stage of the analyzed cases, all of the points show a stable condition. After that when the echoes disappeared, a dry condition was observed except on Kapingamarangi. Actually a large cloud cluster was in the dissipating stage at this point and the assumption made is that the outflow from that dissipating large cluster triggered the echo to form. The moisture field of the GANAL (Global Analysis) analysis supported this assumption (not shown).

3.3 Case 3 : Case study on December 19, 1992 in Manus Island

a) Characteristics of the echo cells

During the study period (December 19), three echoes named Case A, Case B, and Case C appeared in HUML radar coverage and moved NE with a speed of about 5 m/s. The upper panel of Fig. 9 shows the echo area and the lower panel shows the rainfall amount. The threshold of 25 dBZ was used to divide convective and stratiform components for both area and rainfall. The use of 25 dBZ (HUML radar) is different from 40 dBZ (for Keifu Maru radar) depending on the strength of the radar reflectivity. Both area and rainfall amount show three peaks corresponding to three cases. Durations of Case A, Case B, and Case C were 0100-0530 GMT, 0530-1145 GMT, and 1145-1415 GMT (out of radar range) respectively. Each echo consisted of a number of echo cells such as A1, A2, A3 for Case A and B1, B2, B3 for Case B as shown in Fig. 10. This figure represents the target cells A3 of Case A (upper panel) and B1 of Case B (lower panel) respectively. These two cells were analyzed in detail.

As shown in Fig. 11, the RHI scan shows the target cell A3 which is identified at the azimuth of 55° and at 14 km from the radar site at 0157 GMT (upper panel). At this time, it was 4 km in height and 11 km in width (at surface) having a strong reflectivity core at its center. After 43 minutes a new cell was formed at the 3 km level (lower panel) when the cell A3 was going to die down. A strong updraft and convergence zone was positioned at the location of the new cell (not shown). However the main focus of this case is not the formation mechanism of the new cell, but as previously mentioned, to understand the vertical structure of the cloud and the estimation of precipitation in

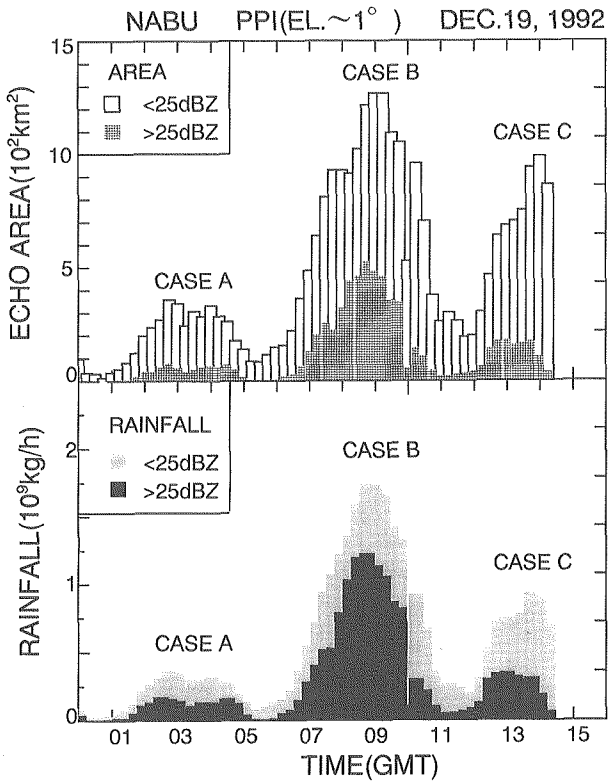

Fig. 9. Time sequences of the echo area (upper panel) and rainfall amount (lower panel) on Dec. 19, 1992 at Nabu in Manus Island. The threshold reflectivity 25 dBZ is used to divide high and low intensity regions and corresponding rainfall amounts. Three echoes named Case A, Case B and Case C are successively appeared in the radar coverage.

comparison with the result of CST analysis.

b) Parameters of cell A3

There are five successive RHI scans to calculate the echo top height, height calculated from Doppler velocity pattern as cloud top height, intensity, and precipitation of the cell A3. The time series of the RHI scans are labeled by the numbers 1, 2, 3, 4 and 5 as shown in Fig. 12. The upper panel shows that the echo top height decreased slowly with the increase of reflectivity at the early stage (1, 2 and 3). It decreased rapidly with the increase of reflectivity at the later stage (4 and 5). On the other hand, the strength of reflectivity decreased slowly with the increase of height below freezing level (~4.5 km). It decreased

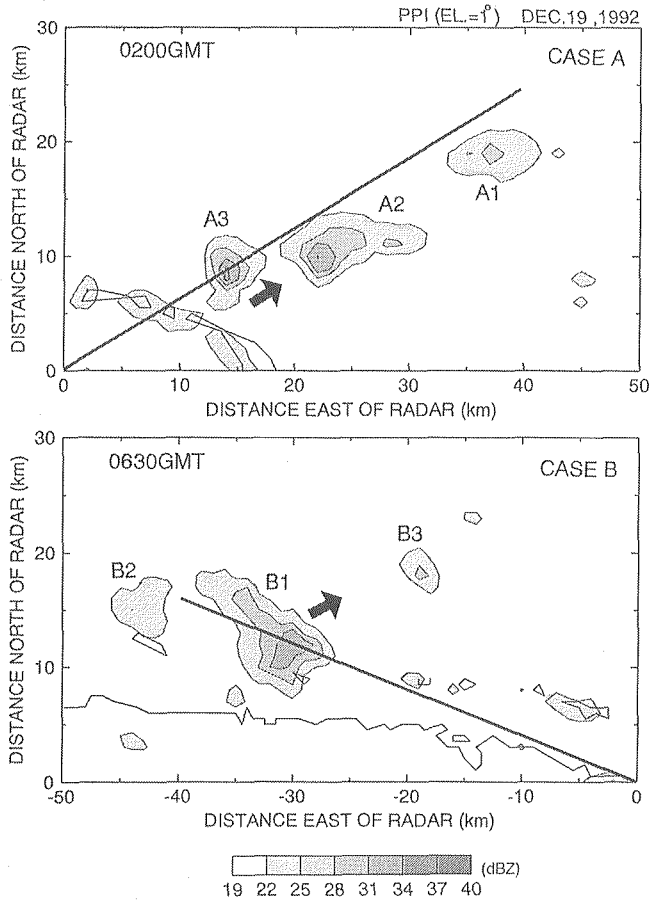

Fig. 10. The PPI images of HUML radar for Case A (upper panel) and Case B (lower panel). The target cells are A3 of Case A and B1 of Case B. Bold solid line represents along which the RHI scan was pointed and the arrow indicates the echo movement direction.

rapidly with the increases of height above the freezing level. These results suggest that below freezing level, high reflectivity results from the existence of convective cumulus towers. And above the freezing level, low reflectivity results from the existence of a deep layer of anvil clouds. These results show consistence with the results of Zipser and Lutz (1994). The lower panel shows that the precipitation rate (PR) increased with the increase of threshold reflectivity at the early stage (1, 2 and 3) and the rate decreases with the increase of threshold reflectivity at the later stage (4 and 5). One can find that the echo top height

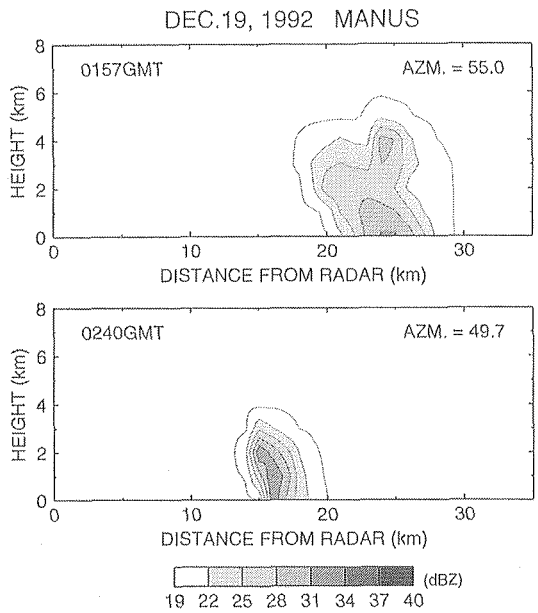

Fig. 11. The RHI images of cell A3 at 0157 GMT (upper panel) and 0240 GMT (lower panel).

started to decrease after stage 4 (upper panel) and PR started to decrease after stage 3 (lower panel). These imply that tropical clouds are tall and intense in the early stage; after that they become weak before the descending in height. In the dissipating stage of cell A3 (4 and 5), the increase rate of PR was higher above threshold reflectivity 28 dBZ in relation to the formation of a new cell (lower panel of Fig. 11).

As represented in the upper panel of Fig. 13, the separation of height calculated from Doppler velocity and echo top height increased with time. This indicates that the cloud expanded its area in the upper-level with time. In the lower panel, the precipitable water (PW) shows that the convective component were dominant at the early stage and stratiform components were dominant at the later stage. These common features of tropical clouds exist here in a single cell. In this case, the PW was calculated from the vertical integration of the PR for a core. The threshold of 25 dBZ and 28 dBZ was used to divide convective (C) and stratiform (S) components.

c) Parameters of cell B1

In cell B1 of Case B, the formation of a new cell (not shown) above the 2 km level was analyzed when cell B1 was in the dissipating stage. The parameters

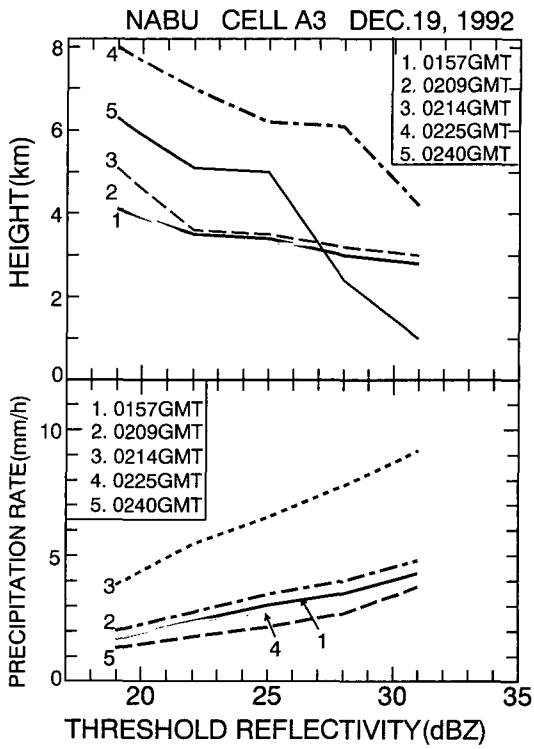

Fig. 12. Comparison of the height (upper panel) and precipitation rate (lower panel) versus threshold reflectivity of cell A3 of Case A. The numbers 1, 2, 3, 4 and 5 are the time series of the RHI scans.

of cell B1 were almost the same as cell A3, as is shown in Fig. 14. Here we see that there were two peaks of the echo top height. The first peak (0641 GMT) appeared when cell B1 was in the mature stage, and the second peak (0712 GMT) belonged to the formation of new cell.

3.4 Comparative study by radar and CST analyses

a) C-band conventional radar and the CST

To better understand the properties of the cloud in a cloud cluster, comparative studies on the SLL echo were performed by using radar and satellite data. Since the analyzed SLL echo is one of the parts of a large system (Fig. 5), hereafter it is called the sub-system (SS ; (Mori, 1992)).

For simplicity, only the SS area identified by radar is superimposed with the CST identified total area as shown in Fig. 15. In the radar analysis, solid (>40

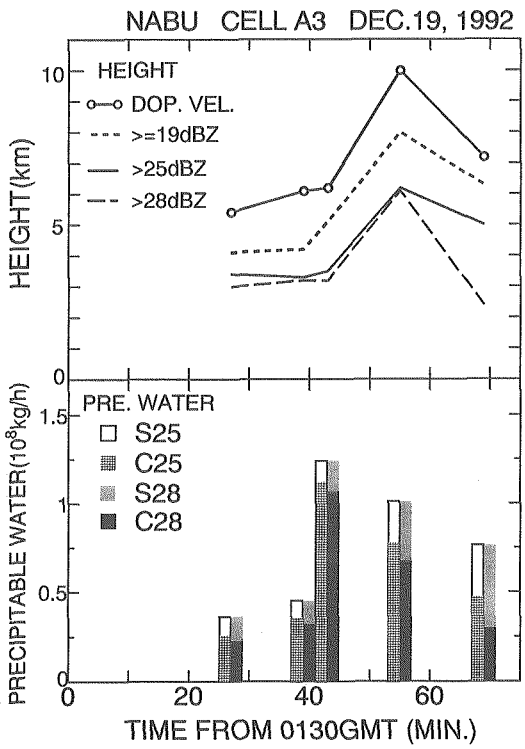

Fig. 13. Comparison of the height (upper panel) and precipitable water (lower panel) versus time of cell A3 of CASE A. The letters S and C represent stratiform and convective respectively. The threshold reflectivities of 25dBZ and 28dBZ are denoted by 25 and 28 respectively.

dBZ) and dashed ($\leq$40 dBZ) lines represent convective and stratiform components respectively. In CST analysis, dark and light shades represent convective and stratiform components respectively. It is seen that in the early developing stage, the CST cannot identify the SS well because the satellite cannot detect the low-level individual shallow convective cloud. In the mature stage, the CST can identify the similar regions of the SS as well as radar can, even though there is a shift between the two positions. It is possible that this shift comes from a systematic error in the GMS data processing or from the difference between vertical structure in the lower and upper troposphere (Houze, 1977; Zipser, 1988). However, the CST can identify the cloud structure when it is well developed. In the dissipating stage, the SS interacted with the other SSs and formed the complex structure as shown in Fig. 15 at 0400 GMT on November 12.

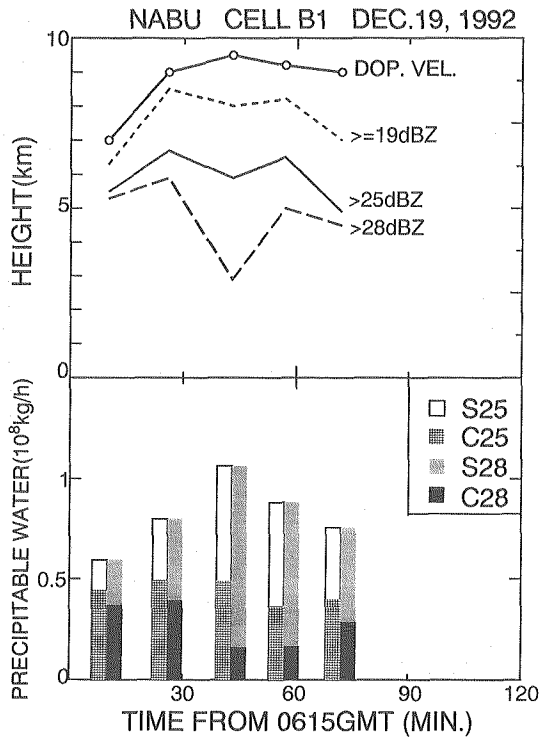

Fig. 14. Same as Fig. 13 except for cell B1 of Case B.

The signature of this type of interaction is helpful in understanding the formation of large-scale cloud clusters which are often observed in the western equatorial Pacific ocean.

The upper panel of Fig. 16 represents the SS areas calculated by radar (R) and the CST (G). The CST could not detect any cloud components untill 2143 GMT on November 11. After that time, the convective area (Rc) identified by radar was comparable with the convective area (Gc) identified by the CST. As expected, after 0043 GMT on November 12, the stratiform area (Gs) identified by the CST was higher than the stratiform area (Rs) identified by radar, because the anvil cloud was formed. On the other hand, the time-integrated convective rainfall (lower panel) amount (Gc) identified by the CST was much lower than the time-integrated convective rainfall amount (Rc) identified by radar. This lower estimation of Gc underestimates the total CST rainfall amount (lower panel) even though the area (upper panel) was comparable.

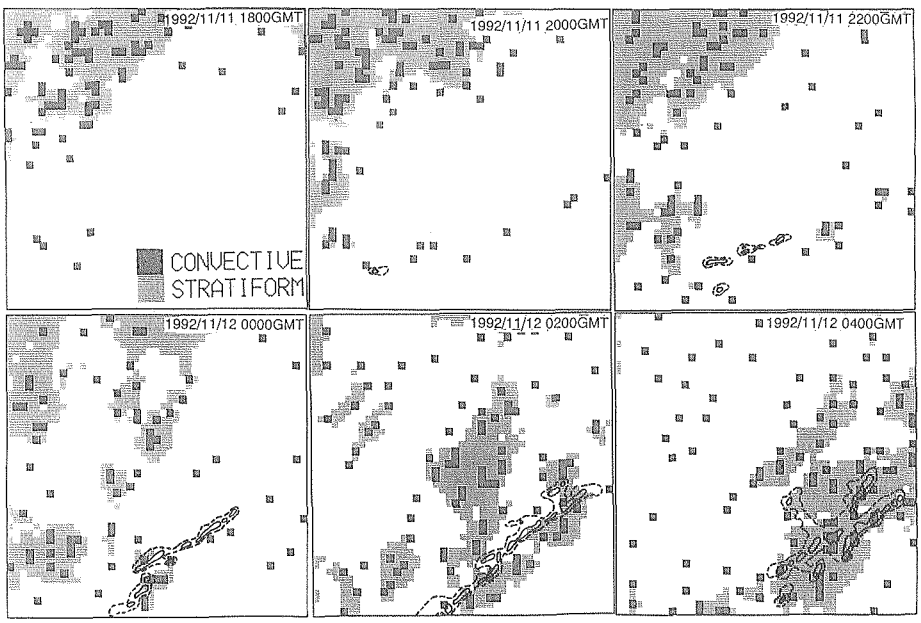

Fig. 15. Time change of the sub-system of radar echo is superimposed with CST determined total regions from 1800 GMT on Nov. 11 to 0400 GMT on Nov. 12, 1992. Radar echo contours are for 20dBZ (dashed) and 40dBZ (solid line). The light and dark shades are for CST determined stratiform and convective components respectively.

The upper panel of Fig. 17 shows the total area calculated by radar (R) and the CST (G). The convective area determined by radar was comparable with the convective area determined by the CST. Both stratiform areas determined by radar and the CST were also comparable. Hourly rainfall amount of total echo (lower panel) again shows an underestimation of the convective rainfall amount (Gc) determined by the CST. The lower estimation of the total rainfall amount (G) determined by the CST was due to the underestimation of the Gc. The area of both radar and the CST analyses are comparable but the rainfall estimated by radar disagrees with the rainfall estimated by the CST. A similar disagreement between the rainfall amounts calculated by radar and the CST is reported in Kikuchi and Uyeda (1996). Therefore, it is essential to find the source of the disagreement between the rainfall amounts determined by radar and the CST. Prior to checking the CST algorithm, we decided to calculate rainfall amounts using Doppler radar data and then compared the rainfall amounts with that of the CST.

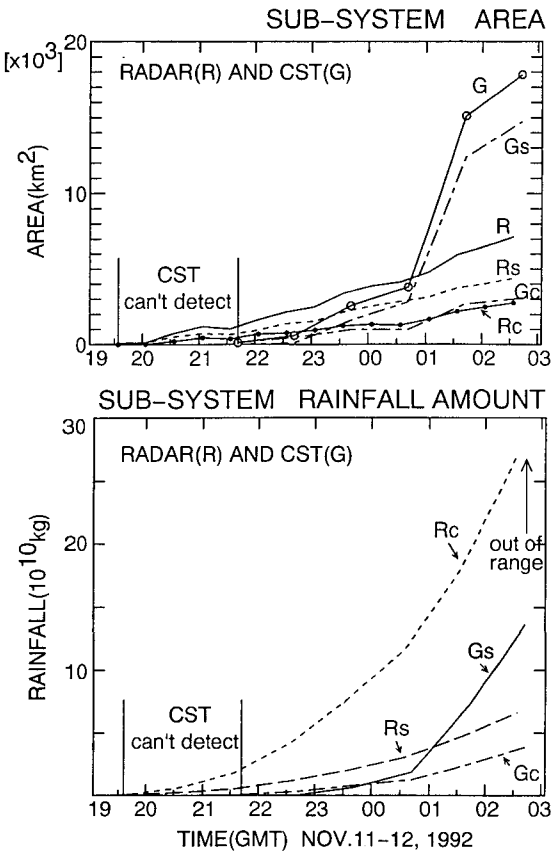

Fig. 16. Time sequence of the comparison between the areas determined by radar (R) and CST (G) analyses for sub-system (upper panel). The subscripts s and c represent stratiform and convective respectively. The lower panel represents the time-integrated rainfall amounts.

b) X-band Doppler radar and the CST

As discussed above, the CST identified area was reasonably comparable to that of the Keifu Maru radar. However, in estimating convective rainfall, either the CST underestimated or the radar overestimated. At present there is no confirmation for which result is the appropriate one. To justify the results of radar and the CST, and to understand the vertical structure of the cloud, analysis was performed on the HUML Doppler radar data in this subsection. It should be noted that there was no Doppler radar data in early November, 1992; a Doppler radar case on December 19, 1992 was chosen.

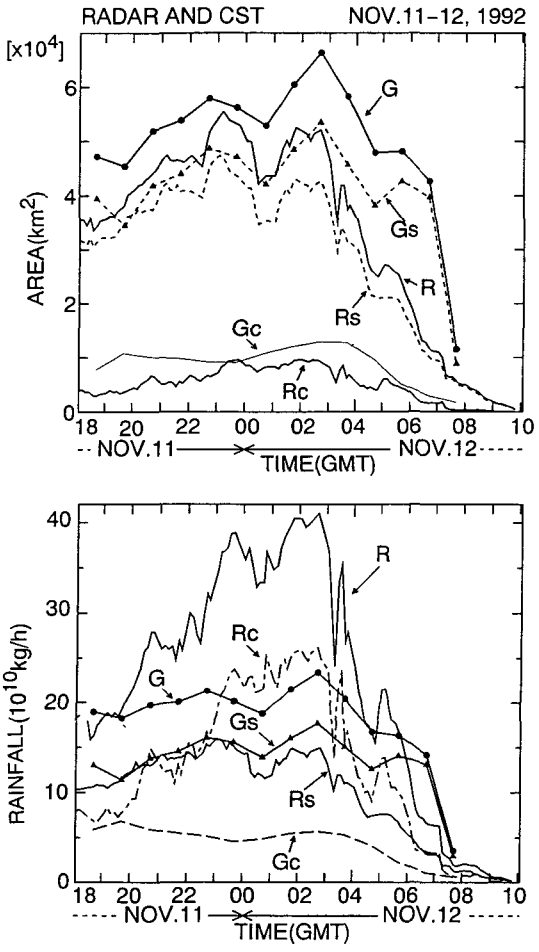

Fig. 17. Same as Fig. 16 except for total echo. The lower panel represents the hourly rainfall amounts.

In the Doppler radar analysis, rainfall amounts determined by the *HUML* radar and the CST are shown in Fig. 18. Qualitatively, patterns were almost the same while the quantity of the CST value calculated was roughly one order higher than that of radar. Here the difference was approximately one order even though the ATI was similar. This gross difference may come from the difference in the rain rate of both radar and the CST analyses. Here again we see the contradiction between the results of radar and the CST in the calculation of rainfall amounts. This demonstrates the necessity of identifying the source

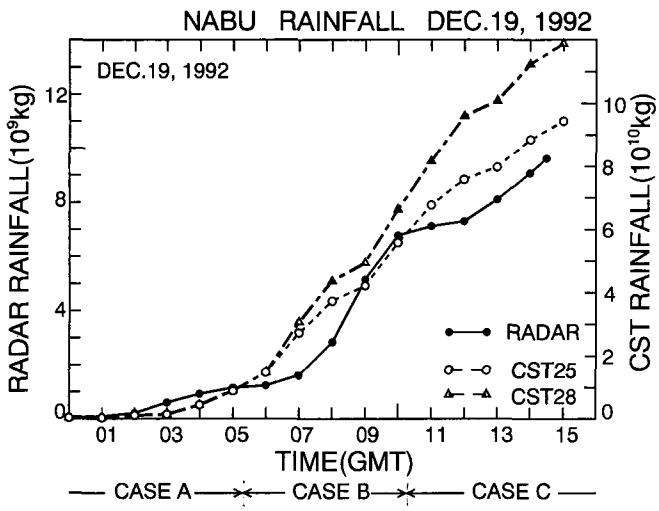

Fig. 18. Time sequence of the rainfall amounts estimated by radar and CST analyses. The meaning of CST 25 and 28 are same as Fig. 13.

of this difference in order to get the value reasonably expected for this region i.e., application of the CST for the TOGA-COARE convection is questionable, without appropriate modification.

4. Discussion

The present work attempted to analyze the Keifu Maru radar data, Doppler radar data and GMS-IR data with the objective of clarifying the characteristics of the tropical clouds and cloud clusters in and around the IFA region during the TOGA-COARE IOP. As was already pointed out, it is very important to reveal the many aspects of cloud properties in the western Pacific oceanic warm pool. It is also necessary to study the interaction between the clouds and cloud clusters in order to determine the organization and maintenance of the MCSs. Furthermore, the quantity of convective and stratiform precipitation is important in itself as well as in showing intimate relationship with water budget, estimation of imported moisture and the determination of sea surface temperature. On the basis of the present analytical results, all of the above properties are thoroughly discussed here.

Table 1. Characteristics of the echoes analyzed on November 11-12, 1992. Echo elements are labeled in the same way as described in the text. Time, horizontal scales, speeds and traversed distances of the echoes and elements were decided subjectively.

	NAME	DETECT TIME (GMT)	DIMENSION IN LENGTH (km)	MERGE TIME (GMT)	SEPERATE TIME (GMT)	DISAPPEAR TIME (GMT)	LIFE TIME h : m	SPEED (m/s)	MAXIMUM DIMENSION (km)	TRAVERSED DISTANCE (km)
CASE-1	a1	21 : 12	~23	···	···	02 : 19	5 : 07	5~12		
	a2	21 : 12	~13	22 : 19	···	···	0 : 52	5~12		
	a3	21 : 48	~25	22 : 27	···	···	0 : 39	6~11		
	a4	21 : 48	~16	22 : 42	···	···	0 : 54	3~12	LENGTH	
	b1	22 : 04	~23	22 : 34	···	···	0 : 30	~6	~110	
	b2	22 : 04	~23	22 : 27	···	···	0 : 23	~6		~155
	a5	23 : 08	~13	00 : 04	···	···	1 : 00	6~11	AREA	
	f1	···	~28	···	23 : 42	00 : 19	0 : 37	···	6.5×10^3	
	f2	···	~13	···	00 : 27	00 : 48	0 : 21	9~12	km^2	
	f3	···	~37	···	01 : 34	02 : 04	0 : 30	···		
	f4	···	~46	···	01 : 34	02 : 19	0 : 45	10~23		
CASE-2	a1	19 : 04	~ 8	···	···	out of range	8 : 30+	5~12		
	a2	20 : 12	~20	07 : 12	···	···	2 : 00	5~12		
	b1	20 : 05	~15	09 : 04	···	···	3 : 44	5~12	LENGTH	
	a3	20 : 48	~10	01 : 28	···	···	4 : 40	5~12	~340	
	b2	22 : 12	~10	23 : 19	···	···	1 : 07	6~11		~350
	a4	23 : 34	~53	01 : 43	···	···	2 : 09	5~11	AREA	
	f1	···	~55	···	00 : 19	out of range	2 : 23+	5~16	7.2×10^3	
	f2	···	~68	···	02 : 42	06 : 00	3 : 18	5~14	km^2	
	f3	···	~45	···	03 : 04	04 : 27	1 : 23	5~14		

4.1 Properties of echo cells and echoes

The details of the echo properties of Case 1 and Case 2 are shown in Table 1. This table can be used to summarize both isolated and nonisolated (i. e., SLL) echoes and their elements. The dimension (in length) was used at identification (new cell) or separation (fragment) time. The life time was calculated from the identification and merging time for the new cell and from the separation and disappearing time for the fragment. In general, the life time of elements in Case 1 was shorter (21 minutes-1 hour) than those of Case 2 (1.07-4.40 hours). The speed of the individual element was calculated during its lifetime. The traversed distance of the long-lived echo was more than two times longer than that of the isolated short-lived echo. The difference between the traversed distance of the two cases was caused by the difference in lifetimes of the elements in their individual cases. The life time of the individual echo element and traversed distance by the echo represent the basic difference between the two types of echo even though the areas and moving speed are almost the same.

The merging criterion is schematically illustrated in Fig. 19. Here two echo cells have to move either in a parallel or an inclined way. They have to change their direction or speed (slow) just before merging. The consecutive distance between the two echoes will be ≥5-7 km. A new cell has to be born in the NE or SW flank of the main echo. The formation of new cell in the NE flank which merges with the main echo is found as an exceptional and new characteristic of the tropical cloud. Usually in the mid-latitudes of northern hemisphere, new echoes are born in the south flank and merge with the main echo. However, the formation of a new cell in both the SW and NE flanks were analyzed. A suitable location for the formation of a new echo depends on the

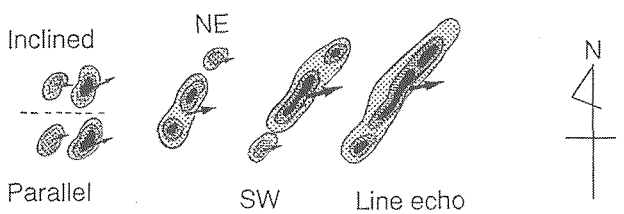

Fig. 19. Schematic illustration of the merging criterion. The symbols NE and SW represent for northeast flank and southwest flank respectively. The arrows indicate the echo movement direction and strong reflectivity regions are shown by dark shade.

flow field of the low-level ambient air. The analysis domain covers both sides of the equator (Fig. 1) where the Coriolis force is negligibly small and the low-level wind field is symmetric to the line perpendicular to the line echo. This equal condition of wind field in both sides of the line echo makes the locations of SW and NE flanks suitable for the formation of new cell. During the formation period (Nov. 11-12) of these two analyzed cases, there was a large cloud in the dissipating stage which partially covered the Keifu Maru region. Inspection of sounding and GANAL (Global Analysis) data supposed that outflow from the dissipating large cloud triggered the formation of the new cells which were organized to develop Case 1 and Case 2.

A detailed analysis of the nonisolated SLL echo and isolated quasicircular echo revealed the time duration of the developing stage. We found that the time duration of the developing stage was about one-third (1/3) of the total lifetime of the echo. This result is well consistent with that of Young et al. (1995) who used ship observation data. This information may be useful in the parameterization of cloud modeling.

To understand the cloud properties in the lower and upper troposphere, radar and satellite data were examined comparatively. Using the superimposed images of radar and CST identified areas, it was possible to analyze the interaction between the SSs in the dissipating stage and the growth of new cells in the lower troposphere at the early stage. Interaction occurred between the clouds, resulting in the formation of a cloud cluster.

In order to know the details of the cloud's vertical structure, Doppler radar data was also utilized. Analyzing the Doppler radar data, some common features of the single echo cell of tropical clouds were also confirmed. The features are as follows:

- Precipitable water dominated by convective components is seen in the early stage and stratiform components are dominant in the later stage.
- Both cell top height and cell intensity are maximum in the early stage.
- Cloud top height is maximum at the beginning of the mature stage and the maximum height is about 17 km (see Fig. 23).

4.2 Intrinsic properties of tropical clouds

The area of the sub-system (SS) was separated (as accurately as possible) by using 7.5 minute interval Keifu Maru PPI (elevation=0.0°) scan data. It was found that the SS covers a small portion of the total echo area and the fractional coverage was 6.5% (0.2%-13.7%) of the total echo area. To clarify the significant behavior of the SS, its area and rain rate are shown in Fig. 20. As

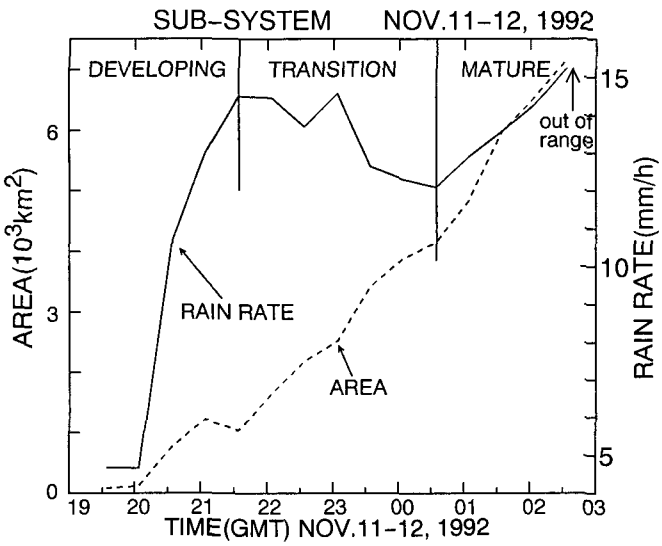

Fig. 20. Time sequences of the echo area and rain rate of sub-system. The solid arrow at 0230 GMT indicates the sub-system is out of radar range.

we see, there are two peaks in the rain rate curve: the first peak appeared at the early developing stage and the second peak appeared when the area reached maximum. The rain rate rose rapidly in the early stage of warm rain as reported by Takahashi and Uyeda (1995). The second peak in the mature stage was during the cold rain when the large anvil cloud developed. During the transition period, the rain rate was inversely proportional to the area due to the merging effect which was related to the formation of the SS. The time duration of the strong rain rate in the developing stage (up to 2325 GMT) was nearly one-third of the total lifetime of the SS. As previously mentioned, the same length (1/3) of the time duration was also found by Young et al. (1995) using ship observation data. Therefore, it may be concluded that the time duration of the developing stage having a strong rain rate will be one-third of the total lifetime of the echo.

To reveal the internal structure of the SS, the convective and stratiform rain rates of both the SS and the total echo are shown in Fig. 21. The capital letters S and R represent the SS and the total radar echo respectively. The small letters c, s, and a, represent convective, stratiform, and average respectively. As we see, the stratiform rain rates for both the SS and the total echo are very close to each other and nearly static. And the convective rain rate (Sc) for the SS was much higher than the convective rain rate (Rc) of the total echo.

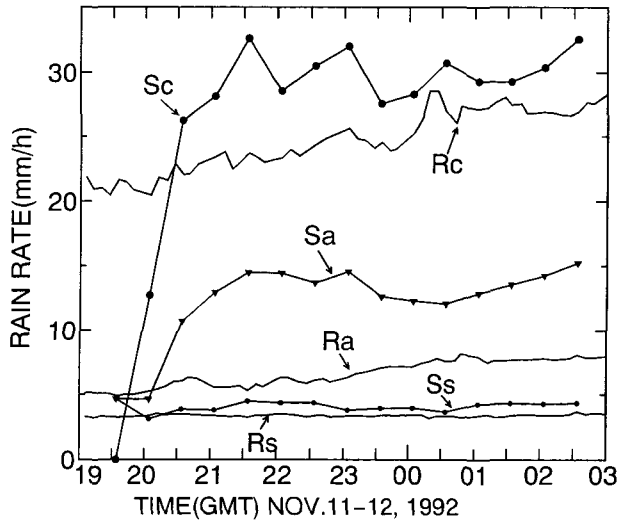

Fig. 21. Time sequences of the rain rate of sub-system (S) and total echo (R). The subscripts are same as Fig. 16. The convective and stratiform component are separated by using 40 dBZ of the threshold reflectivity.

This Sc affected a rise in the average rate ($Sa = 13\ mm\ h^{-1}$) of the SS higher than the average rate ($Ra = 6.5\ mm^{-1}$) of the total echo. Obviously, there is a large difference between Sa and Ra which discloses the necessity of analyzing the characteristics of the individual echo. The increase-decrease-increase nature of Sc implies an important internal structure of the SS : some echo elements are active at a time duration, after that these become weak and the other elements are active. In this way, all of the echo elements play an important role in the maintenance and formation of the cloud. Without extracting the convective component from the average rain rate, it is not possible to reveal this intrinsic property of the cloud structure. This is one of the key advantages of separating convective and stratiform cloud components. It also shows that the production of the stratiform components is from the convective components i.e., the close relationship between the two components : convective and stratiform.

4.3 Cause of the disagreement between the results of radar and the CST

As discussed in section *3.4*, the rainfall amounts calculated by the CST disagree with that of radar. As a quick check, the rain rate calculated by Keifu Maru radar (R) and the CST (G) is shown in Fig. 22. It is seen that the convective rain rate (Gc) determined by the CST was much lower than the

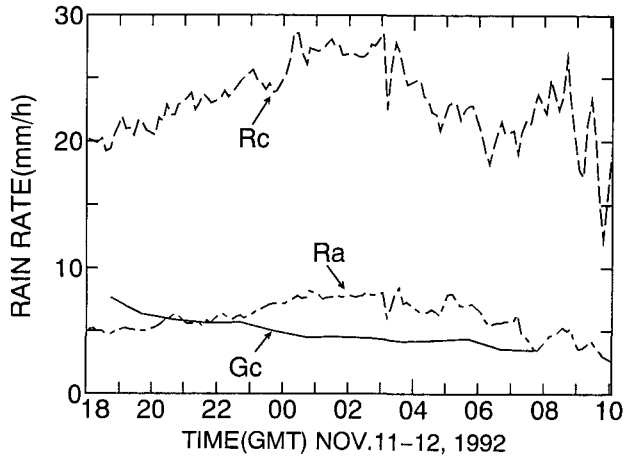

Fig. 22. Same as Fig. 17 except for rain rate. The subscript a represents average.

convective rain rate (Rc) determined by radar. Surprisingly, Gc was also lower than the radar determined average rain rate (Ra). This fact clearly indicates that there is some trouble in the calculation of rain rate either by radar or by the CST. Radar is usually used as ground truth data and Keifu Maru radar has been used to analyze tropical clouds (Mori, 1992 ; 1995). To convert the radar reflectivity into rain rate, one of the standard Z-R relationships derived by Marshall and Palmer (1948) was chosen. Because of this, the calculation of the rain rate in the CST algorithm needed to be checked as was modified for WMONEX, not for the TOGA-COARE domain. Prior to checking the CST algorithm, to ascertain the trouble in the calculation of convective rain rate by CST, the results of the CST were checked with those of Doppler radar.

Before it was possible to declare that the rain rate was uniquely responsible for the large difference in rainfall amounts calculated by radar and the CST, it was decided that the cloud top height in the study region be checked. Figure 23 represents the comparison of cloud top height in the study region (MANUS) and that used in the original CST algorithm (FLORIDA and OKLAHOMA). The curves for Florida and Oklahoma are drawn by using the data of Table 1 respectively, as utilized by Adler and Mack (1984). They calculated these values from model output by using sounding data. AN88 derived the original CST algorithm by using the result of the Florida values. GHC90 modified the CST algorithm for WMONEX and adjusted a few parameters for their study case. In the present study region (MANUS), cloud top heights were calculated by using the height calculated from Doppler velocity. Figure 23 shows that

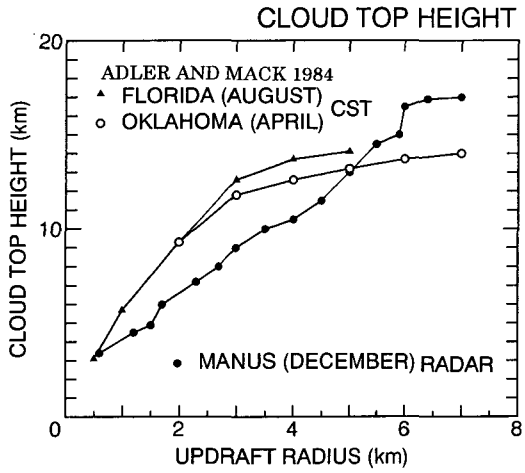

Fig. 23. Comparison of the cloud top height and radius of updraft region in the study region (radar) and the cloud top height used in CST algorithm (CST).

cloud top height in this study region lies below and above cloud top height used in the CST : less and greater updraft radius 5 km. Maximum cloud top height (17 km) of this analysis calculated by radar was the same as the convective cell top height calculated by Leary (1984) for GATE cloud clusters while the maximum cloud top height was 14 km for Florida convection. Therefore, we must assume that this may be one of the causes which has an impact on the calculation of the CST rainfall amount.

It should be noted that the CST convective rain rate related parameters were calculated using a one-dimensional model having some limitations (Stommel, 1947 ; Simpson, 1969 ; Adler and Mack, 1984) and the stratiform rain rate was suggested for use in assigning the radar value. On this point of view, the present study highly recommended the assignment of both convective and stratiform rain rates for the CST analysis from radar data.

Before making the final decision in assigning radar rain rate for CST analysis, it was decided that the present result be checked by using another Doppler radar (ILTS) data which is described here.

The ILTS Doppler radar data collected at Momote on Manus Island was useful in analyzing the same cases (A, B and C) of section 3.3, because Momote is located ~18 km east of Nabu (Fig. 1). For ILTS radar there were some data missing in Case A and Case C. All of the cases, however, should be used to estimate rainfall amount after adjusting the time.

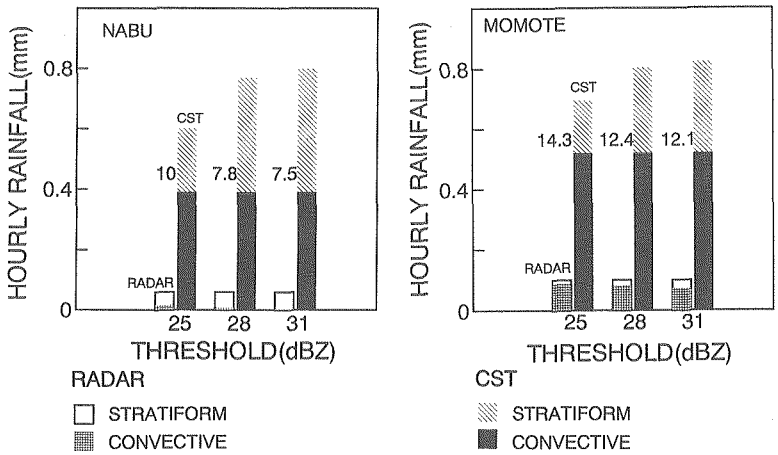

Fig. 24. Hourly rainfall amounts determined by both radar (left column) and CST (right column) at Nabu (left panel) and at Momote (right panel). The legends in this figure show the stratiform and convective components after divided by the threshold 25dBZ.

To analyze the quantitative comparison of rainfall amounts determined by radar and the CST, the rainfall amount was determined using three cases on December 19 as shown in Fig. 24. Convective and stratiform components of both radar and the CST analyses are shown in the legends. For rainfall amounts, the left column is for radar and the right column is for CST while the numbers are their ratios. Here again the large (around 1 order) difference between the rainfall amounts determined by radar and the CST for both Nabu and Momote were analyzed.

The area determined by both radar and CST analyses for Nabu is described in Islam (1996). It was shown that the CST identified regions were twice or three times of the radar echo area. This reconfirms that the rain rate was almost completely responsible in creating the large difference between the rainfall amounts determined by radar and the CST. Therefore, the assignment of the rain rate is essential for a thorough analysis of the radar and satellite data of the TOGA-COARE domain. The assignment procedure is described in a subsequent paper.

5. Conclusions

To understand the properties of the clouds over the western Pacific warm

pool, two cases were studied on November 11-12, 1992 in the IFA region: a quasicircular isolated echo and a squall line-like (SLL) nonisolated echo. Some basic characteristics of the isolated (Case 1) and nonisolated (Case 2) echoes were revealed, such as size, shape, propagation, lifetime, and traversed path. The isolated echo was found to last ~5 hours and its elements lasted from 20 minutes to 1 hour. In contrast, the nonisolated echo lasted ~13 hours while its elements lasted from ~1 hour to ~5 hours. Inspection revealed that the developing stage of the echo lasted almost one-third of the total lifetime. These time durations are important to the model parameterization. It should be noted that the CST was deduced for mature and dissipating stages of the cloud. Therefore, information about the developing stage is absolutely essential in revealing the complete life history of the tropical clouds.

Through the above analysis, knowledge of the properties of cloud clusters has been expanded. Merging of clouds which lasted several hours, were organized to form the MCS. Interaction occurred between the clouds themselves to form the cloud clusters, i.e., cloud clusters are composed of several MCSs. Merging was analyzed in the developing stage and interaction between the subsystems was analyzed in the dissipating stage. The formation of new echo cells were found in both NE and SW flanks and were then found to merge with the main echo.

Since the MCSs were composed of both convective and stratiform components, it was necessary to separate them in radar and satellite images. A threshold reflectivity of 40 dBZ was used for Keifu Maru radar to separate convective and stratiform cloud components. This threshold skillfully separated the areas of the cloud components to conform well with the result of satellite analysis.

However, the total rainfall amount determined by the CST was an underestimate due to the lower estimation of the convective rainfall amount determined by the CST. This points to the necessity of adapting the CST for the TOGA-COARE convection. In order to solve this problem, improvement of the CST algorithm is essential for the TOGA-COARE convection. To adapt the CST for TOGA-COARE domain, modifications are strongly suggested in the: (1) calculation of the slope parameter; (2) determination of the stratiform threshold temperature; and (3) assignment of both convective and stratiform rain rates from radar analysis. Future work will include the modification of the CST algorithm for TOGA-COARE convection, which will be described in a subsequent paper, to obtain better agreement between the rainfall amounts determined by the CST and radar.

Acknowledgments

The authors would like to express their thanks to the JMA for providing Keifu Maru radar data. Special thanks to Dr. N. Takahashi of Communication Research Laboratory, Mr. O. Kikuchi of Japan Air System, Dr. R. Oki of Tokyo University and Mr. M. Katsumata of Hokkaido University for help in data reading. Thanks are extended to Dr. Y. Takayabu of the National Institute for Environmental Studies for providing GANAL data and TCIPO (TOGA-COARE International Project Office) for providing sounding data. Thanks are also extended to Manus radar observation group for providing radar data. During this study, one of the authors M.N. Islam was supported by the Japanese Government (Monbusho) Scholarship from the Ministry of Education, Science, Sports and Culture of Japan.

References

Adler, R.F. and A.J. Negri, 1988. A satellite infrared technique to estimate tropical convective and stratiform rainfall. J. Appl. Meteor., **27**, 30-51.

Adler, R.F. and R.A. Mack, 1984. Thunderstorm cloud height-rainfall rate relations for use with satellite rainfall estimation techniques. J. Clim. Appl. Meteor., **23**, 280-296.

Goldenberg, S.B., R.A. Houze, Jr. and D.D. Churchill, 1990. Convective and stratiform components of a winter monsoon cloud cluster determined from geosynchronous infrared satellite data. J. Meteor. Soc. Japan, **68**, 37-63.

Houze, Jr., R.A. and A.K. Betts, 1981. Convection in GATE. Rev. Geophys. Space Phys., **16**, 591-576.

Islam, M.N., 1996. Characteristics of the tropical clouds and cloud clusters and radar adjusted satellite rainfall estimation during the TOGA-COARE IOP. Doctorate thesis, 153 pp. Graduate School of Sci., Hokkaido Univ., Japan.

Kikuchi, O. and H. Uyeda, 1996. Doppler radar observations on the structure and characteristics of tropical clouds during TOGA-COARE IOP in Manus, Papua New Guinea: Characteristics of cloud clusters analyzed with Doppler radar and GMS-IR data. J. Fac. Sci. Hokkaido Univ., Ser. VII (Geophysics), **10**, 107-133.

Leary, C.A., 1984. Precipitation structure of the cloud clusters in a tropical easterly wave. Mon. Wea. Rev., **112**, 313-325.

Marshall, J.S. and W.M. Palmer, 1948. The distribution of raindrops with size. Jour. Meteor., **5**, 16-18.

Mori, K., 1992. Internal structure and time evolution of a cloud cluster in the western tropical Pacific region observed by Keifu Maru. J. Meteor. Soc. Japan, **70**, 1111-1123.

Mori, K., 1995. Equatorial convection observed by research vessel Keifu Maru during the TOGA COARE IOP, November 1992. J. Meteor. Soc. Japan, **73**, 491-508.

Satoh, S., A. Kinoshita and H. Uyeda, 1995. Doppler radar observations on the structure and characteristics of tropical clouds during TOGA-COARE IOP in Manus, Papua New Guinea: Dual-Doppler analysis of mesoscale convective systems composing a cloud cluster. J. Meteor. Soc. Japan, **73**, 443-459.

Simpson, J. and V. Wiggert, 1969. Model of precipitation cumulus towers. Mon. Wea. Rev.,

97, 471-489.

Stommel, H., 1947. Entrainment of air into a cumulus cloud. J. Meteor., **4**, 91-94.

Uyeda, H., Y. Asuma, N. Takahashi, S. Shimizu, O. Kikuchi, A. Kinoshita, S. Matsuoka, M. Katsumata, K. Takeuchi, T. Endo, M. Ohi, S. Satoh, Y. Tachibana, T. Ushiyama, Y. Fujiyoshi, R. Shirooka, N. Nishi, T. Tomita, H. Ueda, T. Sueda and A. Sumi, 1995. Doppler radar observations on the structure and characteristics of tropical clouds during the TOGA-COARE IOP in Manus, Papua New Guinea — Outline of the observation —. J. Meteor. Soc. Japan, **73**, 415-426.

Webster, P.J. and R. Lukas, 1992. TOGA COARE : the coupled ocean-atmosphere response experiment. Bull. Amer. Meteor. Soc., **72**, 1481-1505.

Young, G.S., S.M. Perugini and C.W. Fairall, 1995. Convective wakes in the equatorial western Pacific during TOGA. Mon. Wea. Rev., **123**, 110-123.

Zipser, E.J., 1977. Mesoscale and convective-scale downdrafts as distinct components of squall line structure. Mon. Wea. Rev., **105**, 1568-1589.

Zipser, E.J., 1988. The evolution of mesoscale convective systems : Evidence from radar and satellite observation. Tropical rainfall mesearements, J.S. Thenon and N. Fugono, Eds., A. Deep Publ., Hampton, Virginia, USA, 159-166.

Zipser, E.J. and K.R. Lutz, 1994. The vertical profile of radar reflectivity of convective cells : A strong indicator of storm intensity and lightning probability ?. Mon. Wea. Rev., **122**, 1751-1759.